

Anatomical, Physical, and Mechanical Parameters of Clone Plantation Tree, *Cunninghamia lanceolata*

Yuanhe Li, Chao Li, Yi Song, Yu Guo, and Lihong Yao *

Anatomical characteristics of the plantation tree, *Cunninghamia lanceolata* were studied. Clonal variability and intra-tree variation, as well as its possibilities of application to the wood industry were analyzed for four clones. Tracheid length from the first to 17th annual ring within clones increased rapidly at first, and then plateaued. The maximum value appeared at the 14th annual ring of clone IV (3795 μm), and the minimum value appeared at the 1st annual ring of clone I (849 μm). Tracheid width and tracheid double wall thickness increased first and then tended to be flat or slightly decreased; tracheid length to width ratio showed an overall increasing trend; the variation of tracheid double wall thickness was not significant. Between clones, the variation coefficient of tracheid width, double wall thickness, and wall to cavity ratio were large. The tissue proportion within clones from large to small was the following: tracheid proportion > wood ray proportion > parenchyma proportion, and there was no significant difference between clones. The basic density within clones showed a gradual increase but a certain fluctuation; the difference between clones was not significant. The maximum crystallinity appeared in clone II (sapwood 55.1%, heartwood 51.2%), and the difference between clones was not significant.

Keywords: *Cunninghamia lanceolata*; Tracheid morphological characteristics; Tissue proportion; Basic density; Crystallinity; MOR; MOE; Tensile test of wood veneer; Timber-variability

Contact information: College of Material Science and Art Design, Inner Mongolia Agricultural University, Hohhot 010018, P.R. China; *Corresponding author: yaolihong82@163.com
Yuanhe Li and Chao Li contributed equally to this work.

INTRODUCTION

Cunninghamia lanceolata is a subtropical tree species, mainly distributed in China and a small part in Vietnam. Within the territory of China, *C. lanceolata* is most widely distributed in the Yangtze River Basin and the south of Qinling Mountains, mainly in Zhejiang, Guangxi, Fujian, Hunan, Guizhou, Jiangxi, Guangdong, Anhui, Sichuan, and Hubei provinces; Jiangsu, Henan, Shanxi, and Yunnan also have a small distribution. *C. lanceolata* has wide distribution, fast growth, and high economic value in China. The cultivation of its plantation has made great contributions to alleviate the shortage of wood resources in China. The new individuals produced by clonal *C. lanceolata* breeding can maintain the inherent characteristics of excellent varieties, and the traits of the offspring are highly consistent. The growth period and growth are relatively uniform, which is convenient for directional cultivation. It is also beneficial to improve wood quality, to save labor, and to increase yield by clonal breeding of *C. lanceolata*. There are significant differences among different clones of *C. lanceolata*. The excellent characteristics of clonal *C. lanceolata* with fast growth and strong resistance are increasingly prominent. The production process of *C. lanceolata* in clonal plantation has been relatively mature. The typical practice is to cultivate small and medium diameter timber and modify the material

to compensate for the lack of large diameter timber and high-quality timber in current forest resources.

The diseases endangering *C. lanceolata* plantation mainly include the sudden fall of seedlings and anthracnose. The former can be prevented by spraying 0.1% sodium p(dimethylamino)benzenediazo sulfonate or 0.5~1% ferrous sulfate solution, and the latter can be prevented by ditching and soil cultivation, clearing diseased branches, deep turning and tending, and interplanting green manure. *Semanotus bifasciatus* is the main pest of *C. lanceolata* plantations. It can be sprayed with 40% omethoate EC 100 ~ 200 times, and injected with dichlorvos 300 times into the wormhole, and then sealed with yellow mud to poison the larvae entering the xylem. The wood of plantation *C. lanceolata* can be used for construction, bridges, shipbuilding, pillars, stakes, poles, furniture, and wood fiber industry raw materials, and its market demand is huge. In the wood-based panel industry, plantation *C. lanceolata* wood can be used to manufacture Glulam, Cross-laminated timber (CLT), Block board, Laminated Veneer Lumber (LVL), Oriented Strand Board (OSB), and Oriented Strand Lumber (OSL). The timber of *C. lanceolata* plantation is of great significance to make up for the serious shortage of large diameter timber of forest resources, and it has great potential in the application of wood-based panel industry.

With the reduction of natural forest resources in the world, plantation timber as an important raw material has become the focus of many researchers. In addition to the plantation of *C. lanceolata*, other tree species of plantation wood research work have certain enlightenment to this study. In one study, sawn boards from a fiber-managed plantation *Eucalyptus globulus* resource in Australia were tested to investigate the recovery rate, visual characteristics, and flexural properties to the extent of utilizing the resource effectively in structural applications and establishing the relevant allowable stress values. Recovery rate of the boards (%) equals the volume of the boards before the final planning stage calculated by measuring the cross-sectional area and length of the boards (m^3) divided by the volume of the harvested logs (m^3) (Derikvand *et al.* 2018). Moreover, fiber-managed plantation *Eucalyptus nitens* resource that was managed to produce woodchips was analyzed to develop higher-value structural products from plantation eucalypt timber that could create new markets for such plantation resources (Derikvand *et al.* 2019). Both unthinned and unpruned plantation *Eucalyptus nitens* and *Eucalyptus globulus* were used in the evaluation of three-ply cross-laminated timber (CLT) floor panels; research has found the flexural performance of CLT panels from *E. globulus* is higher than that of *E. nitens* (Pangh *et al.* 2019).

The nature of plantation trees is affected by the initial planting density, thinning intensity, soil type, cultivation method, and fertilization treatment. Moreover, variability also affects plantation trees, causing great inconvenience to wood quality management and its processing and utilization. Variability is a key issue in the drying of hardwood timber, the mechanical properties, and the correlations with basic density and diffusion coefficient (Watt and Trincado 2019). The initial moisture content that are measurements of variability have been reported by analyzing *Eucalyptus pilularis* within-tree and between-trees from northern New South Wales in Australia (Cabardo *et al.* 2006, 2007). The variability of the properties, such as density, modulus of elasticity, and bending strength, is normally analyzed in a linear mixed model with relative tree size and log type as fixed effects, and with site and tree as random variables (Vestøl *et al.* 2012). Also, modelling the distribution of the variability of timber's mechanical properties will improve its value and lead to more reliable designs (Pommier *et al.* 2014). As a natural unidirectional fiber composite, the considerable variability in mechanical properties of timber is both random and spatial and

is usually referred to as “random spatial variability”, which is most likely to influence the response of structural elements made of clear timber (Moshtaghin *et al.* 2016). To analyze the spatial variability of above-ground biomass (AGB), stocks of managed forests, linear (LM), generalized additive (GAM), and Random Forest (RF) empirical models, with variables related to forest management, stand structure, topography, and climate, are developed to derive spatially explicit estimates and their uncertainty, and compared (Soriano-Luna *et al.* 2018). The variability of *C. lanceolata* mixed with other hardwood forest in southeastern China, which was observed over a period of 15 years (1996 to 2011), has been studied for guiding timber harvesting at different intensities (Wu *et al.* 2018).

The characteristics and variations in the size, shape, and arrangement of various cell types in wood directly affect its properties. In coniferous trees, the total number of tracheids is approximately 90% of the trunk, and tracheids are responsible for the mechanical support and material transport of the tree. Therefore, tracheids largely determine the overall structure and performance of coniferous wood. The morphological characteristics, such as tracheid radial diameter, tangential diameter, and wall thickness, are not only different from each other in different provenances, clones and tree species, but also different from each other in different individuals and parts of the same tree species. Fundamental tracheid morphological characteristics, such as wall thickness (Schimleck and Evans 2004) and length (Hauksson *et al.* 2001; Schimleck *et al.* 2004), are determined by secondary measurement of NIR spectroscopy. Research suggests that NIR spectra correlated with tracheid properties is accurate to develop calibrations for the estimation of density related properties (Jones *et al.* 2005).

Wood tissue proportion is the percentage of all types of cells in cross-section that compose an area, and coniferous wood tissue includes the following: tracheid, longitudinal parenchyma, wood ray, and resin canal. The study of wood tissue proportion is helpful to understand the correlation between wood element and wood properties, which can provide a reliable scientific basis for evaluation of wood quality and rational utilization of wood. Conventional methods of tissue proportion measurement are primarily weighing and grid-counting, and these have the deficiencies of less accuracy, time-consuming, and heavy load for the operators (Yu *et al.* 2009). Technology development allows for digital transverse microstructure images to be photographed through the microscope and video camera; these images are then analyzed using computer image processing techniques to measure wood tissue proportion (Yu *et al.* 2009).

The mechanical and physical properties of wood are important factors used to determine the suitability and application of wood material (Babiak *et al.* 2018). Wood basic density is defined as the ratio of dry matter content to green volume of a sample and is the most widely used indicator of wood quality (Schimleck *et al.* 2018). The wood basic density is easy to measure and has an important influence on the evaluation of wood properties, not only on the mechanical strength of wood, but also on the genetic improvement of wood. Wood basic density is an important indicator of wood physical properties, pulp properties, and pulpwood productivity (Ona *et al.* 1998; Raymond and Muneri 2001; Zhang *et al.* 2011). Basic density is especially appropriate for degraded waterlogged wood that is prone to excessive shrinkage during drying (Passialis 1998). The genetic variation of basic density includes radial and longitudinal variation within-clone, between-clones, different provenances, and different species, of which within-clone variation in basic density is low (Lima *et al.* 2000). Generally, there is some association between basic density and percentage heartwood at the species level, but no association at the provenance within species level (Searle and Owen 2005). In a test of wood basic density

related to nutrient concentration, fertilizer decreased basic wood density 7% at ground level and 5% over the entire stem (Crous *et al.* 2009). Obviously, the measurement of wood basic density is a requirement in many wood-product markets (Deng *et al.* 2014), especially the plantation wood market. Wood basic density can be measured using diverse direct and indirect methods, of which the most common direct method for determination of wood basic density consists of a gravimetric procedure (Vikberg and Elustondo 2015) sampling with a Pressler borer, which results in wood cores that are easy to weigh. The indirect methods include densitometric methods that are based on high-resolution imaging of differences in attenuation of non-visible radiation by the samples investigated (Diesel *et al.* 2014). In addition to these traditional methods, near-infrared spectroscopy (NIRS) has the potential of predicting wood basic density rapidly and nondestructively (Liang *et al.* 2019). In several tests, British Standards and ASTM (American Society for Testing and Materials) standard wood testing procedures are referred by researchers to analyze wood basic density (Sseremba *et al.* 2020).

Wood behaves like an elastic solid when force is applied to it, and therefore modulus of elasticity (MOE) is used to describe the stiffness of wood; in general a high value of MOE implies a high resistance of wood to deformation (Olaoye and Okon-Akan 2020). Scientists conventionally use universal testing machine (UTM) to determine elasticity of wood, and UTM tests are considered expensive, demanding high maintenance cost, and are destructive to samples (Amera *et al.* 2005). Hence, the use of non-destructive acoustic methods (NDAT) is needed. There exist several non-destructive acoustic methods for estimating elasticity of wood based on ultrasound (Wang *et al.* 2003), stress waves, infrared spectroscopy (Bailleres *et al.* 2005), and vibration method (Barrett and Hong 2010; Almeida *et al.* 2014; Guan *et al.* 2019; Olaoye and Okon-Akan 2020). After analyzing anatomical, physical, and mechanical properties of plantation wood, this study considers four strains of clone plantation *C. lanceolata* timber in Kaihua County, Zhejiang Province as the research object. The general rule of plantation *C. lanceolata* properties was analyzed between anatomical, physical, and mechanical characteristics and timber-variability, for guiding plantation wood production, improving the level of management of forestry production and the comprehensive utilization of plantation *C. lanceolata* resource and expanding the application range of plantation *C. lanceolata*, which has practical significance. The objective is also for the plantation *C. lanceolata* wood to simultaneously meet a series of property requirements and to list each of the important properties that likely would be regarded as important for decision-making in wood industry.

EXPERIMENTAL

Materials

Specimens of *Cunninghamia lanceolata* were obtained from Kaihua County tree farm in Zhejiang Province, located at latitude 28° 54' N and longitude 118° 01' E. The region belongs to the subtropical monsoon climate zone with distinct seasons and warm and humid. The average annual temperature is 16.4 °C, sunshine duration is 1712.5 h, frost free period is 252 days, and the year average rainfall is 1814 mm. The four clones, fostered in 1998 and cut down in 2017, were close to each other and grew on the same soil and climate conditions, and the same planting density and cultivation treatments. Each sample tree, one tree per clone, was sawn into segments of 2 m length and the height ranged from 3.5 m to 5.5 m. The basic information of each sample tree is shown in Table 1.

Table 1. Basic Dimensions of Each Sample Trees

Clone Name	Serial Number	Height (m)	Diameter at Breast Height (cm)
Kaihua#3	I	18.0	18.2
Kaihua#13	II	18.0	17.2
F24X-NA-1-1	III	16.2	20.5
Daba#8	IV	18.0	18.1

Methods

The method of tracheid morphological characteristic measurement is as follows: a 3-cm-thick disk was sampled at the bottom of each sample tree segment. Then, from these sample disks, 3 to 5 match-stub-like samples were obtained from earlywood of each annual ring from the southern part of each sample disk. Each match-stub-like sample was placed into a test tube, and distilled water was added; test tubes were then heated in 90 °C water baths for 40 min until the samples moved to the bottom of the test tubes. When the sample sank to the bottom of the test tube, it began to discharge hot air in the test tube. After discharging the air, the sample was put into a mixed solution of the ratio of 30% hydrogen peroxide to glacial acetic acid was 1: 1. The test tube was sealed with the preservative film, and then it was perforated on the preservative film to ventilate. The water bath continued to heat for 2 h until the samples turned white. Then, the samples were rinsed thoroughly with distilled water, and then, using forceps, a small amount of the sample was placed on the microscope slide with a drop of distilled water. The samples were slapped gently with an anatomical needle until the samples were completely dispersed.

After air-drying the samples, an optical microscope was used to observe and measure the intact tracheid in the prepared microscope slide. Tracheid radial diameter was measured at 40× magnification; tracheid tangential diameter and double wall thickness were measured at 400× magnification (light microscope model: SWN-800; Beijing PDV Instrument Co., Ltd., Beijing, China). Tracheid radial diameter and tangential diameter were measured at three positions near the middle of tracheid, and the average value of measured values at the three positions was taken as final tracheid radial diameter and tangential diameter value. For each clone, 80 samples per annual ring were randomly measured, and the average value of tracheid morphological characteristics were taken as final radial diameter value, tangential diameter value, and double wall thickness value of each sample. After the measurement, data was input to Excel software (Microsoft Corp., Excel 2019, Redmond, WA, USA) to calculate the tracheid double wall thickness, length-width ratio, and wall-cavity ratio. Tracheid length to width ratio is equal to tracheid length value divided by tracheid width value; tracheid wall to cavity ratio is equal to the obtained tracheid double wall thickness value divided by tracheid width value.

The test method for determination of tissue proportion consisted of five steps. First, materials were selected by taking a 3-cm-thick disk at the same height of each clone *C. lanceolata*; a small wooden block was obtained from heartwood and sapwood in the 3-cm-thick disk. Second, the wooden blocks were placed in a beaker and heated in a water bath until samples reached the slicing requirements. Approximately 2 to 3 slices each from cross and tangential sections of the sample were cut by LeiCa sliding (LEICA ULTRACUT R; LEICA, Wetzlar, Germany) for later use. The thickness of slices was 18 µm. Third, the slices were stained for 4 h by placing slices in 4% safranin staining solution. Then, the stained slices were gradually dehydrated for 10 min at different ethanol concentrations of 25%, 50%, 75%, 95%, and 100%, respectively. Finally, xylene was used to treat the

samples transparently and seal them with gum. Image analyzer with digital image processing hardware (Model: Quantimet 720; IMANCO, Cambridge, U.K.) was used in conjunction with an optical microscope (Model: SWN-800; Beijing PDV Instrument Co., Ltd., Beijing, China) to measure tissue proportion, and each sample was measured 30 times.

In terms of wood basic density test, the method is adopted as a drainage method according to GB/T 1933 (2009). The specific operation is as follows. First, 2 cm width of small sticks were cut through the pith heart center along the north-south direction at the same height of four clones, and irregular samples were made within each annual ring. Secondly, 17 samples were obtained for each clone; they were numbered and placed in beakers. Distilled water was added to the beaker, soaking the sample more than 1 to 2 cm until it reached a saturated state. The volume of each sample was measured by saturated water method, and then the sample was placed in an oven at 103 ± 2 °C until it was completely dried; the weight of each sample was subsequently measured. The wood basic density is calculated using Eq. 1,

$$\rho_0 = m_0 / V_0 \quad (1)$$

where m_0 is the dry mass of each sample (g), V_0 is the volume of moist wood (cm^3), and ρ_0 is wood basic density (g/cm^3).

The crystallinity was measured using an X-ray diffractometer (Model: Smart Lab SE, Rigaku, Tokyo, Japan). The different clones were sampled according to heartwood and sapwood, and ground into wood powder by a wood powder machine. The powders above 100-mesh were screened and placed in the constant temperature and humidity box to balance the moisture content for two weeks. During the test, the CuK radiation wavelength in the X-ray was 1.54059 Å, the 2θ sweep angle ranged from 3 to 50°, and the scanning speed and step length were 0.02°. Referring to the Segal method, the maximum of diffraction peak near 22° and diffraction peak minima near 18° are mainly obtained during the test, which are calculated according to the relative crystallinity calculation Eq. 2,

$$Crl = (I_{002} - I_{am})/I_{002} \times 100\% \quad (2)$$

where Crl is relative crystallinity (%), I_{002} represents the maximum intensity of lattice diffraction angle, which generally occurs near $2\theta = 22.5^\circ$, and I_{am} is the scattering intensity of amorphous background diffraction near 18°.

According to the maximum peak width value at the crystal surface 002, the D_{hkl} microcrystalline width was obtained by the Scherer formula, Eq. 3,

$$D_{hkl} = k\lambda / (\beta \cos\theta) \quad (3)$$

where D_{hkl} is the grain diameter (nm) perpendicular to the direction of the crystal surface (HKL), λ is the wavelength (0.154 nm), β is the widest peak width of the diffraction 2θ , θ is the diffraction angle, and k is Scherer constant (0.9).

Modulus of rupture (MOR) values of different clones were tested according to GB/T 1936.1 (2009). The specimen dimension was 20 mm × 20 mm × 300 mm (radial × tangential × longitudinal). In the mechanical test, the specimens were evenly placed on two supports of the mechanical testing machine, with a distance of 240 mm between the supports. The loading method was adopted in the center of the specimen, and the loading speed was evenly added with the radial of the specimen in the middle at a speed of 10 mm/min. The MOR is calculated using Eq. 4,

$$\sigma_{bw} = (3P_{\max} l) / (2bh^2) \quad (4)$$

where σ_{bw} is the bending strength when the moisture content of the sample is W (65%) (MPa), P_{max} is the failure load (N), I is the distance between the two supports (mm), b is sample width (mm), and h is the sample height (mm).

Modulus of elasticity (MOE) of specimens was tested according to GB/T 1936.1 (2009). The MOE was calculated using Eq. 5,

$$E_w = (23Pl^3)/(108bh^3f) \quad (5)$$

where E_w is the flexural elastic modulus when the moisture content of the sample is W (65%) (MPa), P is the difference between upper and lower loads (N), I is the distance between the two supports (mm), b is sample width (mm), h is the sample height (mm), and f is the deformation value of the upper and lower load samples (mm).

Tensile test of wood veneer is achieved by using a micromechanical testing machine (Model: 5948; Instron, Norwood, MA, USA). Different clones of plantation tree were prepared at the same height cut a 5-cm-thick disc, through the pith center according to the north-south sawing width of 3 cm center strip, soaked in water for softening, slide cutting in each annual ring's early wood section, each annual ring took 3 pieces of 80- μ m-thick micro-slice samples, placed between two slides. Specimens were placed between two slides and clamped with a rubber band. Specimens were placed in a constant temperature and humidity box with ambient temperature of 20 °C and moisture content of 65%. Specimens were tested after 2 weeks when the equilibrium moisture content was adjusted. In the tensile test, specimens were placed in the fixture of the micro-mechanics testing machine; the width and thickness of the measured wood chip sample were inputted, and the maximum tensile stress value after fracture was tested. The tensile strength of the wood chip was calculated automatically by the computer.

Stepwise regression analysis method was used to analyze the effects of 10 anatomical characteristics on modulus of rupture (MOR), modulus of elasticity (MOE) and wood veneer tensile strength of clone plantation *C. lanceolata*. The regression model was calculated by SPSS 13.0 (IBM, SPSS 13.0, New York, USA).

RESULTS AND DISCUSSION

Analysis of Tracheid Morphological Characteristic Value of Each Clone Plantation *Cunninghamia lanceolata*

The secondary xylem of *Cunninghamia lanceolata* is mainly composed of tracheid cells, whose anatomy plays a fundamental role in the physical and mechanical properties of the tissue (Liu and Zhao 2012). From the microscopic level, the representative anatomical characteristics of *C. lanceolata* mainly include tracheid length, tracheid width, tracheid double wall thickness, tracheid length to width ratio and tracheid wall to cavity ratio (Locosselli and Ceccantini 2012). These special parameters determine the morphology of tracheid at the cellular level (Adey-Johnson *et al.* 2020).

In the paper industry, the longer the tracheid length, the greater the tear resistance, tensile strength, and folding resistance of paper (Liu and Zhao 2012). According to the research, tracheid width is also an important factor affecting the properties of wood pulp, papermaking, and paper. Fibers with large cavity and thin wall are conducive to the formation of paper and the interweaving of fibers (Abdel-Aal *et al.* 2015). Fibers with thick wall and small cavity have high tear strength. Tracheid double wall thickness affects the

strength of paper, and it is also the material basis for affecting wood density and strength-weight ratio. Tracheid length to width ratio is an important factor affecting the performance of wood fiber materials. The larger it is, the more favorable the fiber combination is. It is generally believed that the tracheid length to width ratio greater than 80 can meet the requirements of fiber industry raw materials. Tracheid wall to cavity ratio is the ratio of tracheid wall thickness to lumen diameter (Zhu *et al.* 2006), which is called the Runkel coefficient in the paper industry. According to the Runkel theory, when the ratio is less than 1, the fiber contact area can be increased in the wood processing, thereby increasing the utilization rate of wood, which is helpful for the processing of wood materials belongs to excellent fiber raw materials. On the contrary, when the ratio is greater than 1, it is inferior.

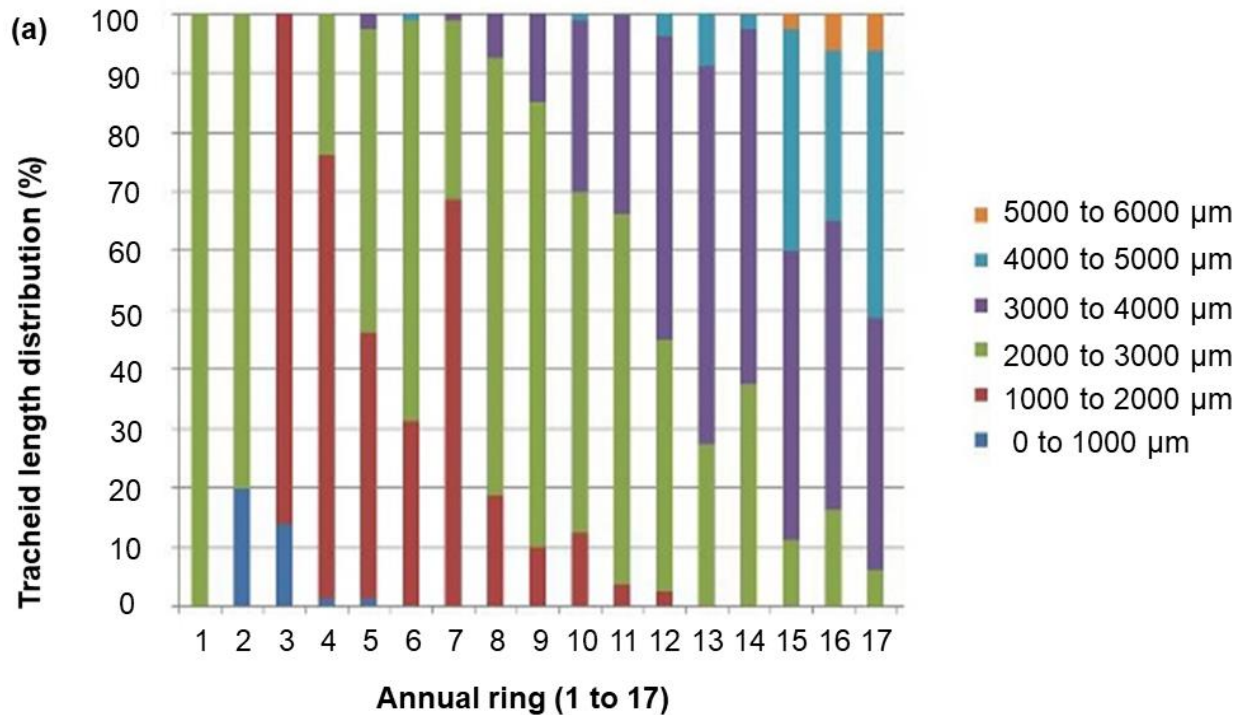
It should be noted that, due to the directional cultivation of clonal plantation cultivation conditions in sufficient water and soil fertility, the formation of earlywood within every annual ring accounted for the majority of the material and thus can be regarded as being more representative (Vaganov *et al.* 2009). Accordingly, its properties can be used to summarize the characteristics of *C. lanceolata* from a relatively macro level on the variability of 1 to 17 annual rings, thus ignoring the variability of earlywood and latewood (Havimo 2010) within annual rings. Among all the anatomical characteristics, tracheid length is the most direct parameter to reflect the tracheid morphological characteristics (Watt *et al.* 2008). Therefore, the tracheid length distribution figure of four clones from 1 to 17 annual rings was specially presented, in order to observe the distribution and variability (Fig. 1).

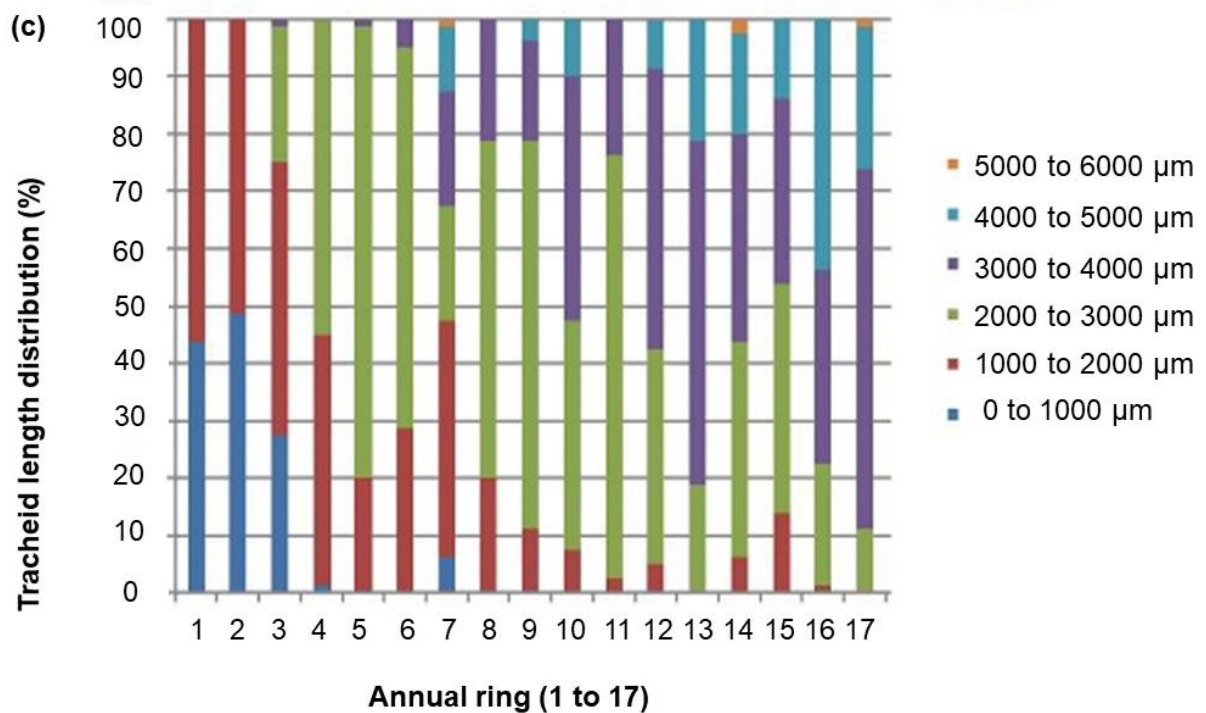
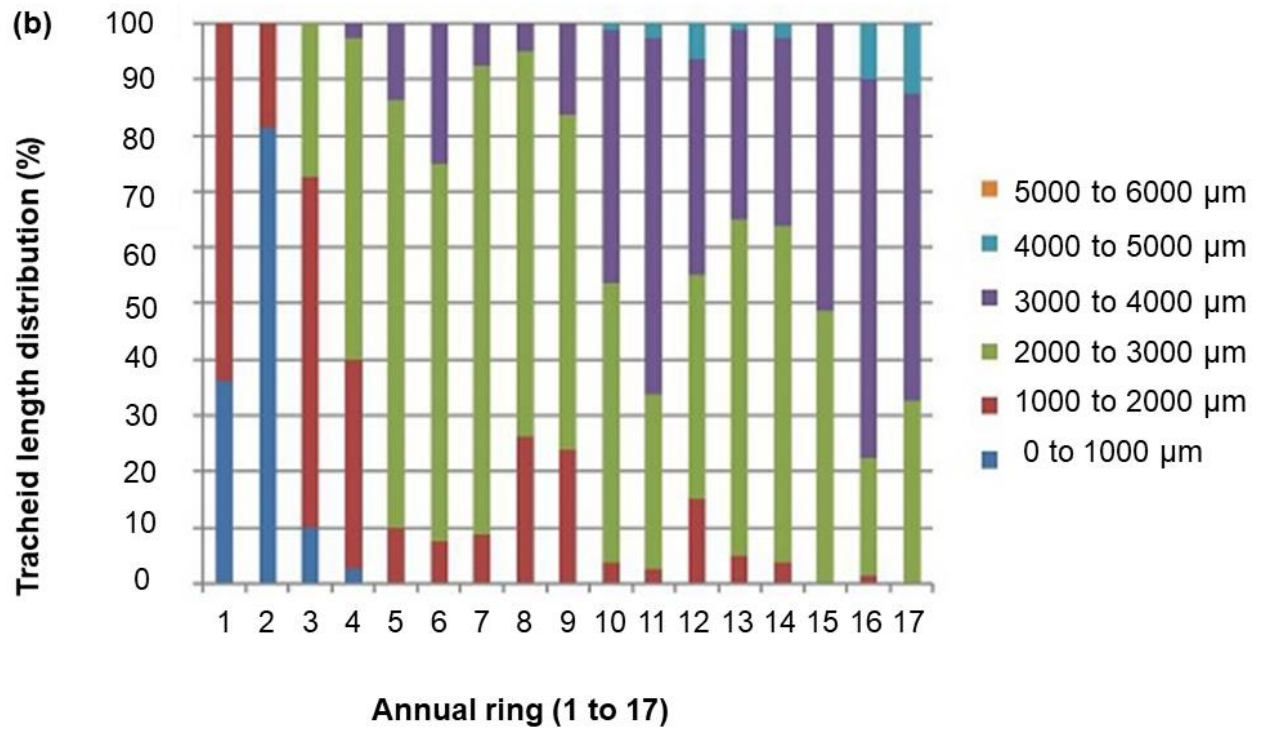
The experimental data showed that the tracheid length showed an overall trend of gradual increase from 1 to 17 annual rings. Only the 1st and 2nd annual ring of clone I showed a longer tracheid length, and then from the 3rd annual ring it began to show the same rule as other clones. This particular tracheid length in the 1st and 2nd annual ring of clone I was due to its rapid maturation in the growth environment during the first and second years. It has been shown that a longer average tracheid length can be associated with more productive ecosites that supported faster growth (Townshend *et al.* 2015). The distribution of tracheid length of clones II, III, and IV showed high similarity from 1 to 17 annual rings, while clone I had certain difference compared with other clones, but the difference was not significant.

Overall, almost all four clones had tracheid length longer than 2000 μm in length from the 3rd annual ring, and more than 3000 μm in length from the 8th annual ring. In addition, the common law reflected by the four clones was the annual ring width gradually decreased while the tracheid length gradually increased from 1 to 17 annual rings, so it can be speculated that there was a significant negative correlation between the tracheid length and the annual ring width.

Pashin and Zeeuw (1980) divide wood fiber and tracheid radial variability-law into three types: type I, tracheid length rises rapidly from pith heart center to bark at first, and then remains horizontal when tracheid length reaches a certain age; type II, tracheid length rises gradually from pith heart center to bark; type III, the tracheid length increases to a maximum and then decreases. In Fig. 2(a)(b)(c) reflected the radial variability of tracheid in clone I. From Fig. 2(a), it can be found that the tracheid length of clone I changed significantly with the increase of annual ring age, showing an overall increasing trend, belonging to type I (Pashin and Zeeuw 1980). The reason for this may be due to the vertical division of primitive cells in the cambium and the intergrowth of daughter cells. The tracheid length of the 1st annual ring was the minimum (849 μm), and the tracheid length

increased rapidly from the 1st to the 6th annual ring. From the 7th to the 17th annual ring, tracheid length showed an increasing trend, but the fluctuation was large and the increasing trend was relatively flat. The maximum value was 3367 μm at the 16th annual ring. This may be due to the growth of trees to a certain time; the primordial cells in the cambium began to mature and became longer, and the primitive cells in the shorter cambium gradually disappeared and produced daughter cells (Yarnan 2007).





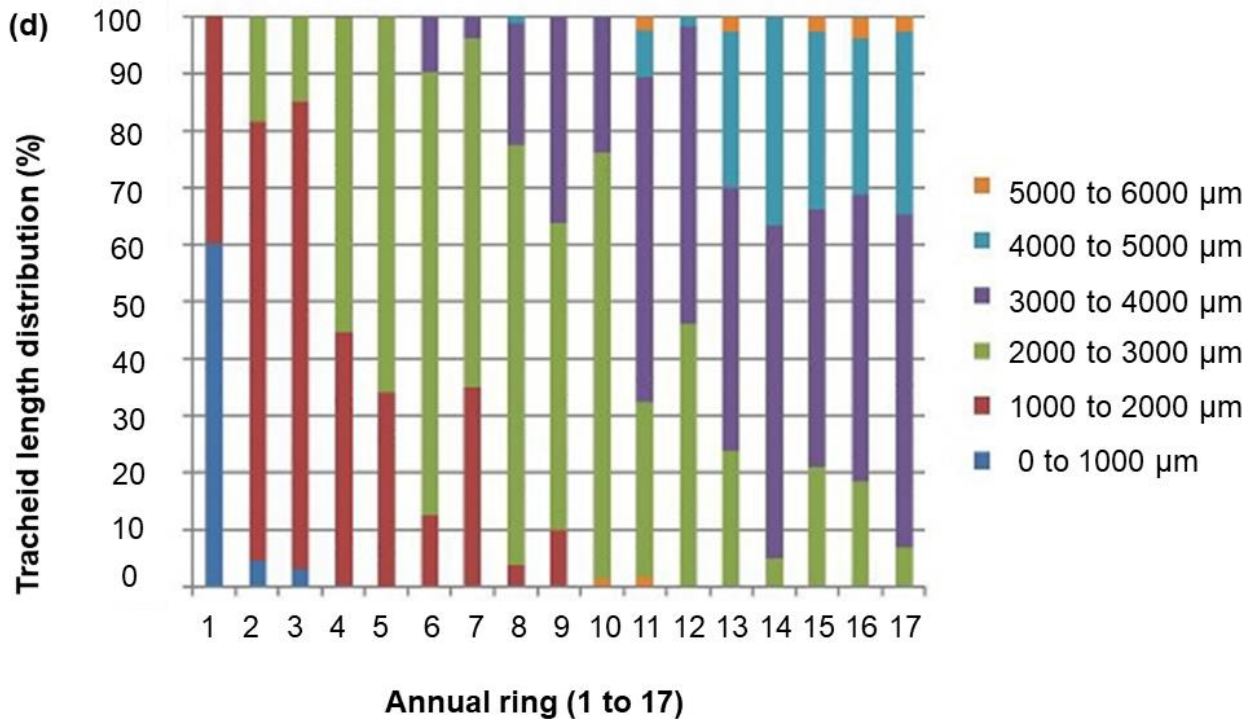
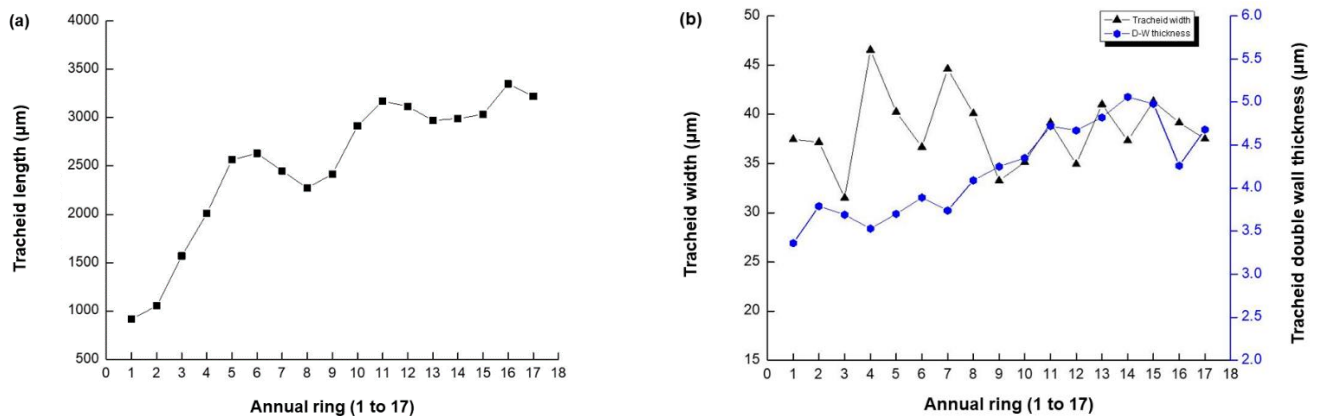


Fig. 1. The distribution of tracheid length in each annual ring: (a): clone I; (b): clone II; (c): clone III; (d): clone IV

According to Fig. 2(b)(c), there was no significant change law in the tracheid width and tracheid double wall thickness from 1 to 17 annual rings. The minimum tracheid width of clone I was 29.96 µm at the 9th annual ring, and the maximum width was 47.22 µm at the 15th annual ring, while the maximum tracheid double wall thickness was 4.98 µm. The values of tracheid length to width ratio and tracheid wall to cavity ratio increased and fluctuated greatly from 1 to 17 annual rings. The minimum value of tracheid length to width ratio was 22.35 at the 1st annual ring, and the maximum value was 117.1 at the 17th annual ring. Interestingly, the mean value of tracheid length to width ratio between the 5th and 17th annual ring was greater than 50.



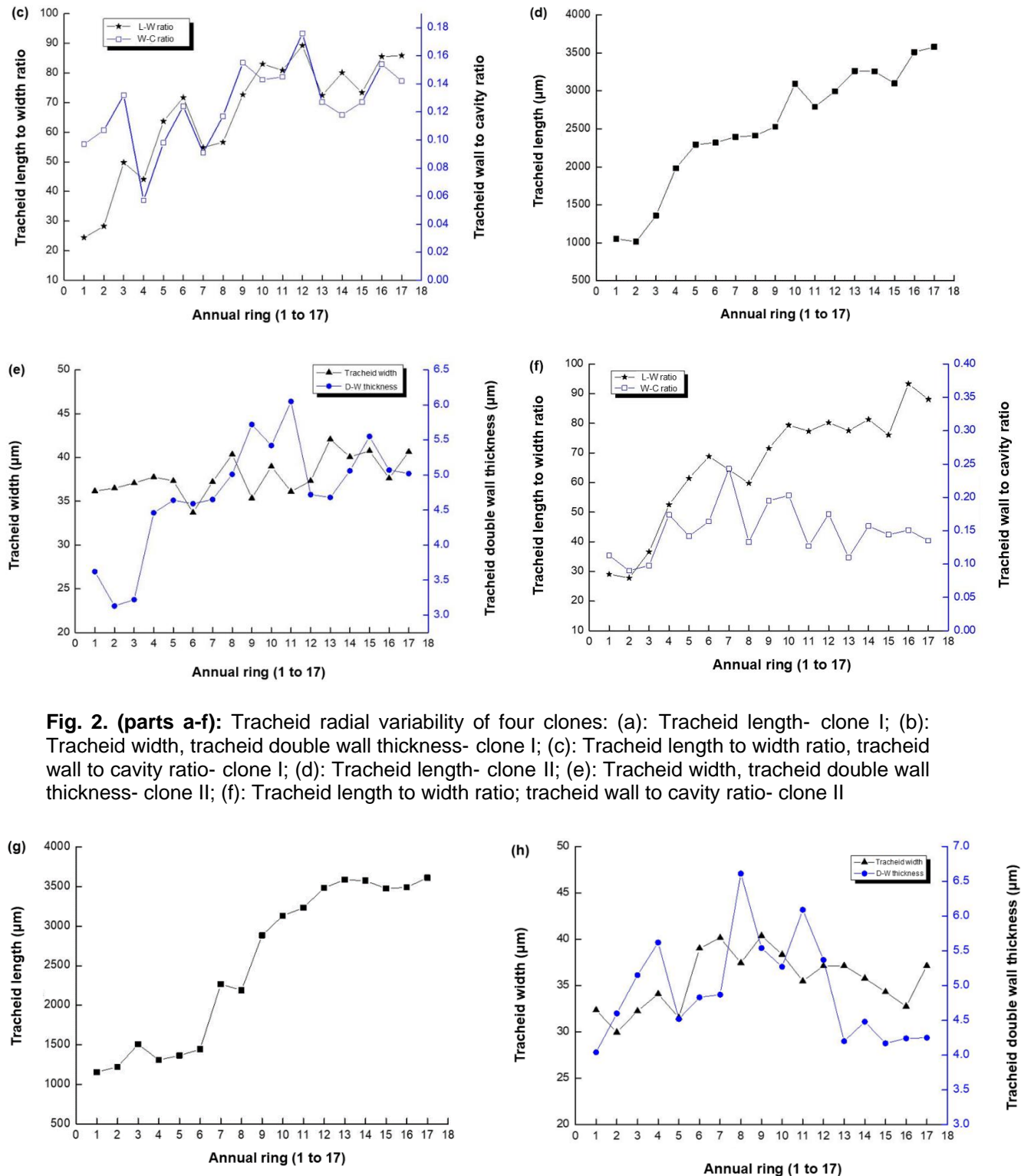


Fig. 2. (parts a-f): Tracheid radial variability of four clones: (a): Tracheid length- clone I; (b): Tracheid width, tracheid double wall thickness- clone I; (c): Tracheid length to width ratio, tracheid wall to cavity ratio- clone I; (d): Tracheid length- clone II; (e): Tracheid width, tracheid double wall thickness- clone II; (f): Tracheid length to width ratio; tracheid wall to cavity ratio- clone II

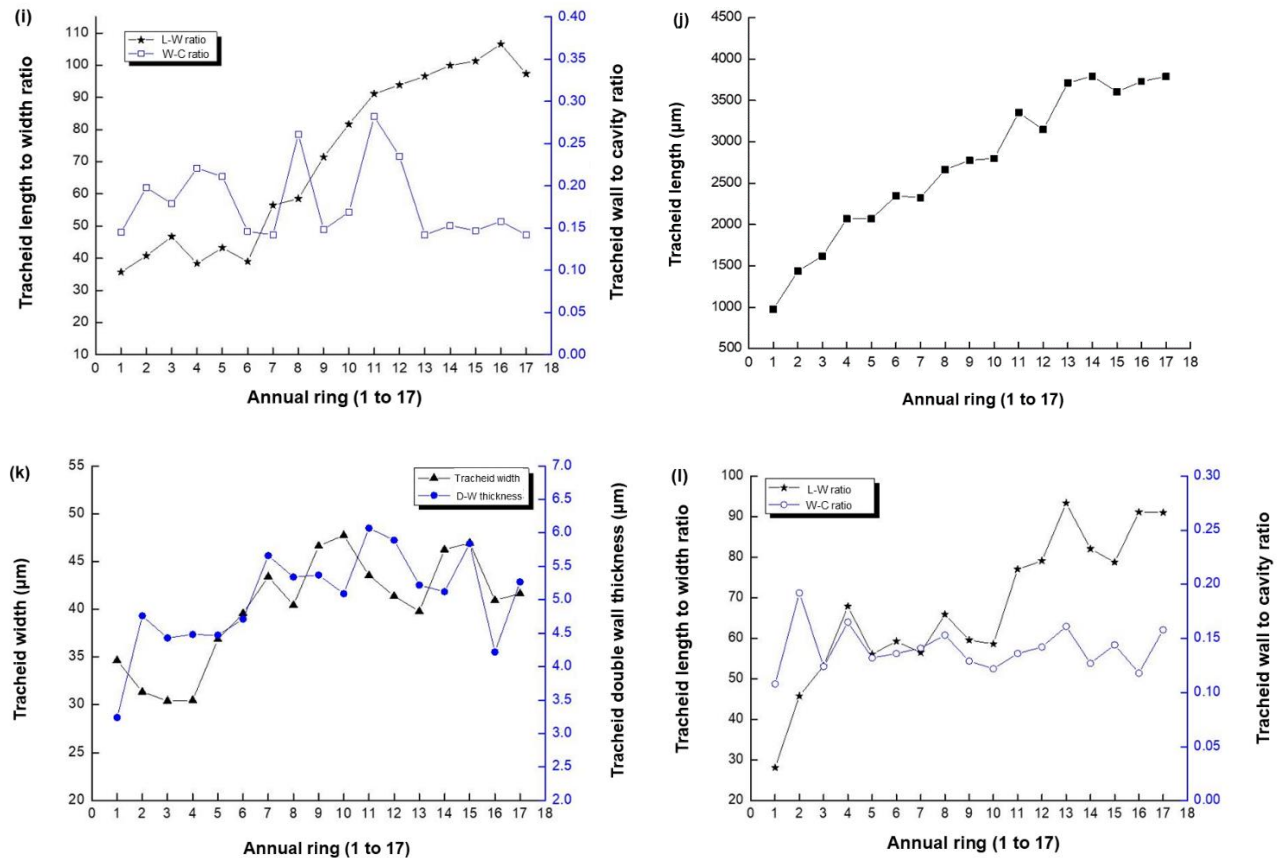


Fig. 2. Tracheid radial variability of four clones: (a): Tracheid length- clone I; (b): Tracheid width and tracheid double wall thickness- clone I; (c): Tracheid length to width ratio and tracheid wall to cavity ratio- clone I; (d): Tracheid length- clone II; (e): Tracheid width and tracheid double wall thickness- clone II; (f): Tracheid length to width ratio and tracheid wall to cavity ratio- clone II; (g): Tracheid length- clone III; (h): Tracheid width and tracheid double wall thickness- clone III; (i): Tracheid length to width ratio and tracheid wall to cavity ratio- clone III; (j): Tracheid length- clone IV; (k): Tracheid width and tracheid double wall thickness- clone IV; (l): Tracheid length to width ratio and tracheid wall to cavity ratio- clone IV

In Fig. 2, parts (d) (e) (f) reflected the radial variability of tracheid in clone II. According to Fig. 2(d), it indicated that the tracheid length of clone II changed significantly with the increase of annual ring age and showed an increasing trend in general. The tracheid length was shorter in the early annual ring age, and the minimum was 1031 μm at the 2nd annual ring. The tracheid length increased rapidly from the 1st to 10th annual ring, and from the 10th to 17th annual ring. The tracheid length increased generally but fluctuated to a certain extent and reached the maximum at the 17th (3758 μm). According to Fig. 2(e), there was no obvious change law of tracheid width with the minimum value (30.1 μm) at the 6th annual ring and the maximum value (50.9 μm) at the 13th annual ring. Tracheid double wall thickness showed an overall increasing trend in the 1 to 11 annual rings. From the 12th annual ring, tracheid double wall thickness started to decrease and then remained stable with the maximum value (6.05 μm) at the 11th annual ring. According to Fig. 2(f), tracheid length to width ratio increased with the increase of annual ring age and reached the maximum value (93.3) at the 16th annual ring. Tracheid wall to cavity ratio from 1 to

17 annual rings showed a trend of first increase and then decrease and fluctuated greatly, the maximum value was 0.243 at the 6th annual ring.

Parts (g), (h), and (i) of Fig. 2 reflected the radial variability of tracheid in clone III. According to Fig. 2(g) the tracheid length changed significantly with the increase of annual ring age and the minimum value was 1155 μm . The tracheid length increased rapidly from 1 to 13 annual rings, and slowed down from 13 to 17 annual rings, reaching the maximum value of 3614 μm at the 17th annual ring. According to Fig. 2(h), the radial variation of tracheid width was first increased and then decreased. The minimum value was at the 3rd annual ring (32.3 μm), and the maximum value was at the 9th annual ring (40.4 μm). Tracheid double wall thickness generally showed a trend of first increase and then decrease, and the maximum value (6.61 μm) appeared at the 8th annual ring. According to Fig. 2(i), tracheid length to width ratio gradually increased and reached the maximum at the 16th annual ring (106.6). There was no obvious variation in tracheid wall to cavity ratio, and the maximum value was 0.282 at the 11th annual ring.

In Fig. 2, parts (j), (k), and (l) reflected the radial variability of tracheid in clone IV. Tracheid length changed significantly with the increase of annual ring age, showing an overall increasing trend and a slight fluctuation with minimum value (977 μm) at the 1st annual ring. Tracheid length increased rapidly from 1 to 14 annual rings, and the increasing trend slowed down from 14 to 17 annual rings, reaching the maximum at 14th annual ring (3795 μm). The radial variation laws of tracheid width and tracheid double wall thickness were similar. With the increase of annual ring age, they generally increased first and then tended to be flat, and the variation coefficient of tracheid double wall thickness was large. The minimum value of tracheid width was at the 3rd annual ring (30.4 μm), and the maximum value was at the 10th annual ring (47.7 μm). The maximum value of tracheid double wall thickness was 6.07 μm at the 11th annual ring. Tracheid length to width ratio gradually increased and reached the maximum value of 93.3 at the 13th annual ring. There was no obvious variation in tracheid wall to cavity ratio, and the maximum value was 0.192 at the 2nd annual ring. Among the four strains of *C. lanceolata*, the average tracheid length ranged from 2369 μm to 2568 μm (Fig. 1). Among the four different clones, the coefficient of variation was greater than 28%, indicating that the value of tracheid length varies greatly in radial direction (Fig. 2).

Under the 0.01 level, the clone of *C. lanceolata* tracheid double wall thickness was influenced noticeably. The value of tracheid double wall thickness from large to small was respectively IV (4.95 μm), III (4.83 μm), II (4.59 μm), I (4.03 μm). The largest value was 22.9% higher than that of the smallest. Tracheid width and tracheid wall to cavity ratio exhibited a remarkable difference between clones ($0.01 < P < 0.05$). Tracheid width value from large to small was: III (38.12 μm), I (36.34 μm), II (35.95 μm), and IV (33.79 μm). The average tracheid width of clone III was 12.81% higher than the minimum value. The variation coefficient of different clones was relatively small and the morphological value of tracheid width is stable.

Average tracheid wall cavity from large to small was: III (0.18) > II (0.15) > IV (0.14) > I (0.12). The variation coefficient of clone I, II, and III were more than 20%, and showed large variations in stability. The range of variations was large and unstable.

Repeatability is an important genetic parameter in tree clone breeding, and it is the proportion of the sum of environmental variance and genotype variance in the expression variance (Ivkovic and Rozenberg 2004). The repeatability was calculated using Eq. 6,

$$h^2 = 1 - 1/F \quad (6)$$

where F is the variance test value.

Because there was no noticeable difference in the tracheid length and the tracheid length to width ratio between clones, one can conclude that the index was less affected by genetic factors, so the estimation of its repeatability was not considered. The repetition force of the tracheid width, the tracheid double wall thickness, and the tracheid wall to cavity ratio were 0.739, 0.774, and 0.618, respectively, all of which were above the medium level. This indicates that these indicators are controlled by genetics above the medium level and could provide a theoretical basis for genetic improvement.

Analysis of Tissue Proportion of Each Clone Plantation *Cunninghamia lanceolata*

Tissue proportion values from large to small represent tracheid proportion, wood ray proportion, and parenchyma proportion, respectively. Based on Fig. 3, the tracheid proportion and parenchyma proportion of heartwood were lower than that of sapwood. This may be due to the relatively small tracheid width and high mean tracheid density at primary growth of plantation. When the plantation becomes mature, primitive cell division in the cambium is stable, and the tracheid proportion and parenchyma proportion increased, which reflects that the moisture and inorganic salt transport capacity of sapwood is relatively strong. Wood ray proportion is affected by tracheid proportion and parenchyma proportion. With the increase of the growth ring age, tracheid proportion increased and wood ray proportion decreased. Moreover, there was no noticeable difference between sapwood and heartwood at the level of $\alpha = 0.05$. According to analysis of variance, there is no noticeable difference in tracheid proportion, parenchyma proportion, and wood ray proportion between the four clones.

Analysis of Basic Density Leading to Radial Variability for Each Clone Plantation *Cunninghamia lanceolata*

According to Fig. 4, the basic density of radial variability for each plantation tree gradually increased and fluctuated to a certain extent above and below the trend line from pith heart center to bark. The minimum value appeared near the 2th annual ring, which is approximately 0.29 g/cm³. The mean basic density of “F24X-NA-1-1 (III)” was lower than the other three plantations with a value of 0.326 g/cm³, while others is approximately 0.335 g/cm³. There was no noticeable difference in the basic density for each plantation tree between clones at the level of $\alpha = 0.1$.

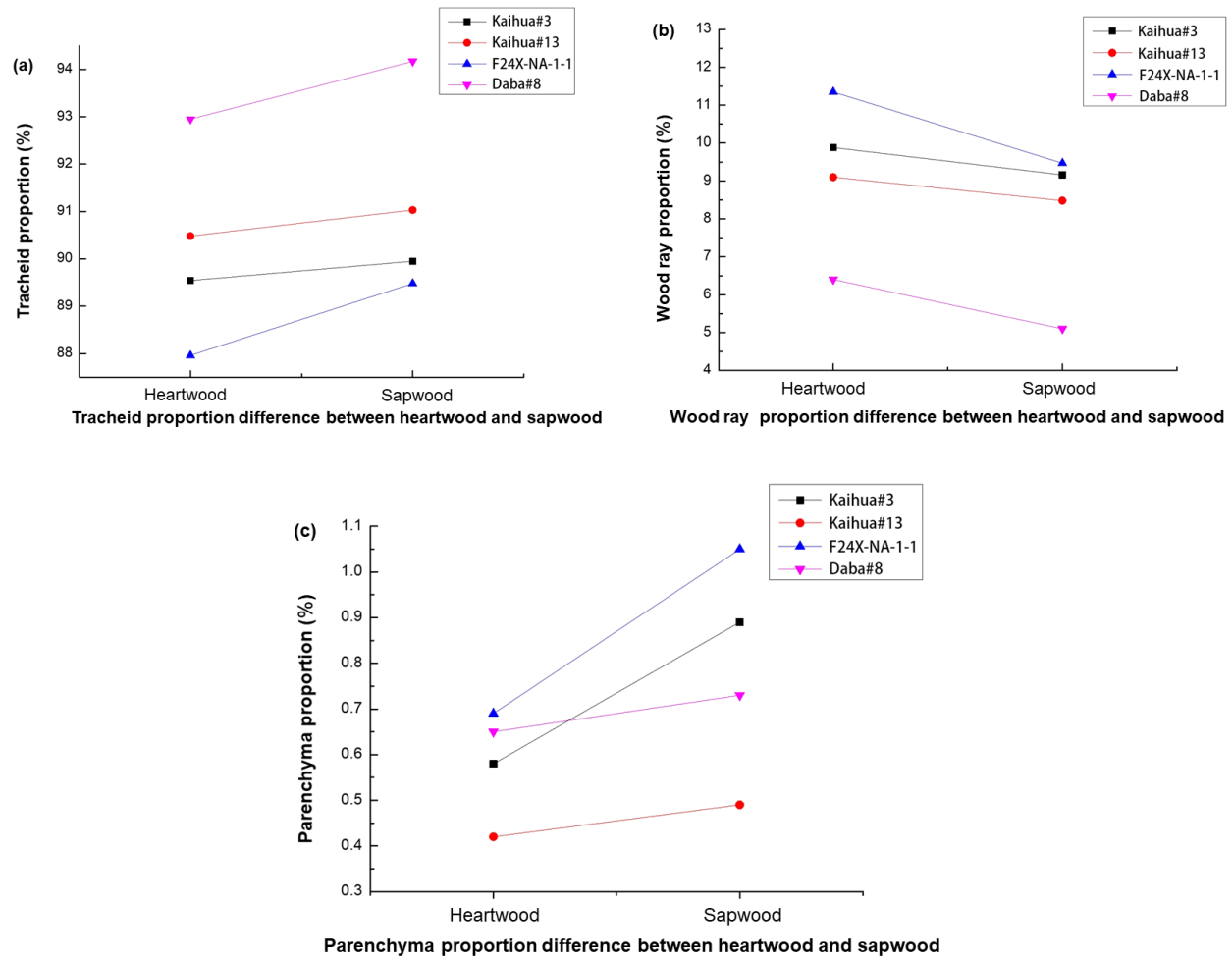


Fig. 3. Discrepancy of tracheid proportion (a), wood ray proportion (b), and parenchyma proportion (c) between heartwood and sapwood

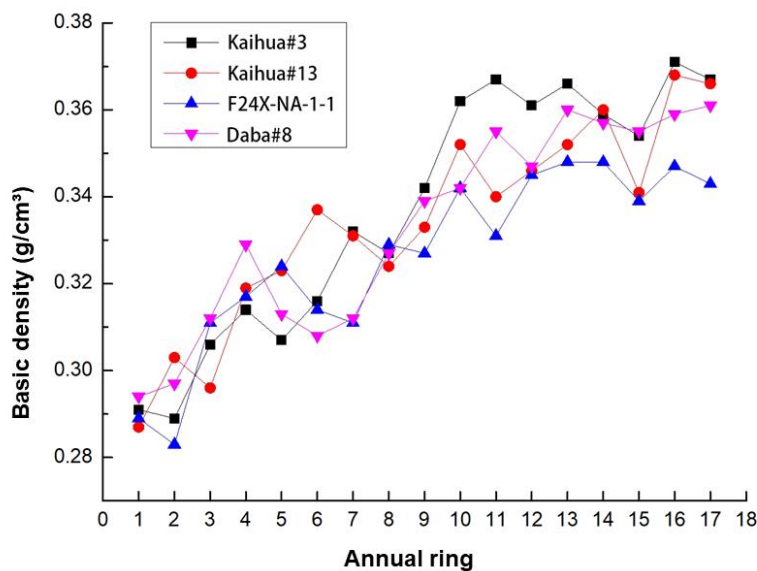


Fig. 4. Radial variation of basic density of each clone plantation trees

Analysis of Crystallinity for Each Clone Plantation *Cunninghamia lanceolata*

According to Tables 2 and 3, the crystallinity of four plantations in sapwood was greater than that of heartwood, and the variation within clone and between clones was not noticeable at the level of $\alpha = 0.1$. The crystallinity is the percentage of crystal area in the whole cellulose. Crystallinity affects the mechanical properties of wood. Relevant studies have shown that crystallinity is positively correlated with wood density, bending strength, hardness, and other indicators, while negatively correlated with impact toughness, moisture absorption, and other properties. Therefore, the variability between clones should not be considered when breeding for the plantation.

Table 2. Comparison of Crystallinity for Each Plantation

Crystallization Position	Clone			
	Kaihua#3 (I)	Kaihua#13 (II)	F24X-NA-1-1 (III)	Daba#8 (IV)
Heartwood	50.99°	51.24°	46.53°	49.26°
Sapwood	53.54°	55.07°	47.58°	53.1°

Table 3. Analysis of Variance for Crystallinity Between Clones

Variative Source	Sum of Square	Degree Freedom	Mean Square	F	P-value	F crit
Between Groups	15.87661	3	15.87661	2.05953617	0.20126274	5.9873776
Within Group	43.61983	4	14.53994	3.142116	0.148839	6.5913821
Total	62.12958	7				

Establishment of Multivariable Regression Equation Among Anatomical, Physical and Mechanical Parameters for Clone Plantation *Cunninghamia lanceolata*

Stepwise regression is a regression function that introduces and removes independent variables step-by-step and reflects the influence degree of multiple independent variables on dependent variables. Stepwise regression analysis of each parameter is made by multivariate regression,

$$y = b_0 + b_1 \times x_1 + b_2 \times x_2 + \dots + b_m \times x_m$$

where independent variables are basic density (x_1), tracheid length (x_2), tracheid width (x_3), tracheid double wall thickness (x_4), tracheid length-width ratio (x_5), tracheid wall-cavity ratio (x_6), tracheid proportion (x_7), parenchyma proportion (x_8), wood ray proportion (x_9), crystallinity (x_{10}), and dependent variables are MOR (y_1), MOE (y_2), wood veneer tensile strength (y_3).

Table 4. Summary of Mathematical Model for MOR

Model	Correlation coefficient R	R ²	Standard error
1	0.718	0.516	3.30478
2	0.792	0.628	2.74633
3	0.886	0.786	2.28379
4	0.911	0.831	1.79195
5	0.946	0.920	1.26221

Table 5. Regression coefficient Table for MOR

Model	Correlation coefficient		<i>t</i>	Significance
	Beta	Standard error		
1 constant	67.713	33.047	-3.572	0.174
Basic density	27.942	2.182	8.679	0.019
2 constants	62.249	31.516	-7.023	0.098
Basic density	26.411	2.019	7.174	0.017
Tracheid proportion	24.036	1.192	3.440	0.038
3 constants	56.091	31.027	-5.193	0.077
Basic density	24.178	1.985	9.181	0.014
Tracheid proportion	21.127	1.063	4.124	0.036
Crystallinity	10.107	0.382	2.686	0.045
4 constants	53.039	30.630	-7.246	0.024
Basic density	23.216	1.779	12.145	0.009
Tracheid proportion	17.142	0.737	7.231	0.027
Crystallinity	8.084	0.338	6.534	0.021
Tracheid wall-cavity ratio	9.328	1.019	13.906	0.010
5 constants	-47.824	21.664	-11.208	0.006
Basic density	17.001	1.045	15.792	0.004
Tracheid proportion	14.237	0.618	9.663	0.006
Crystallinity	7.457	0.180	13.663	0.009
Tracheid wall-cavity ratio	7.420	0.951	11.746	0.011
Tracheid width	2.433	0.617	16.39	0.009

Table 6. ANOVA (analysis of variance) Table for MOR

Model	Quadratic sum	DOF	Mean square	F distribution	Significance
1 regression	24.157	1	24.157	6.108	0.097
residual	27.587	10	3.211		
total	51.744	11			
2 regression	27.104	2	23.627	7.771	0.038
residual	24.640	9	3.079		
total	51.744	11			
3 regression	29.826	3	22.928	9.526	0.027
residual	21.918	8	2.121		
total	51.744	11			
4 regression	32.507	4	22.096	10.123	0.019
residual	19.267	7	1.775		
total	51.744	11			
5 regression	43.808	5	21.904	13.749	0.009
residual	7.966	6	1.593		
total	51.744	11			

According to the regression model (Table 4, 56), it can be concluded that the most effective anatomical parameters to MOR (y_1) include basic density (x_1), tracheid width (x_3),

tracheid wall-cavity ratio (x_6), tracheid proportion (x_7), and crystallinity (x_{10}). Mathematical model concluded is given as Eq. 7:

$$y_1 = 17.001x_1 + 2.433x_3 + 7.92x_6 + 14.237x_7 + 7.457x_{10} - 47.824 \quad (7)$$

Table 7. Summary of Mathematical Model for MOE

Model	correlation coefficient R	R2	Standard error
1	0.734	0.539	279.27
2	0.807	0.651	232.64
3	0.913	0.834	197.47
4	0.942	0.894	178.91

According to Tables 7, 8, and 9, it can be concluded that the most affectable anatomical parameters to MOE (y_2) include basic density (x_1), tracheid length (x_2), tracheid proportion (x_7), and parenchyma proportion (x_8). The mathematical model concluded is given as Eq. 8:

$$y_2 = 4006.679 - 13.52x_1 + 8.44x_2 + 0.504x_7 - 0.17x_8 \quad (8)$$

Table 8. Regression Coefficient Table for MOE

Model	Correlation coefficient		t	Significance
	Beta	Standard error		
1 constant	4855.039	504.311	11.341	0.000
Basic density	-15.341	2.078	3.171	0.009
2 constants	4539.179	425.517	11.795	0.000
Basic density	-13.358	1.795	5.597	0.010
Tracheid length	9.861	1.341	3.79	0.008
3 constants	4318.733	329.849	13.093	0.000
Basic density	-10.748	-1.477	4.079	0.038
Tracheid length	7.352	2.904	2.649	0.016
Wood ray proportion	-0.280	0.058	2.195	0.082
4 constants	4006.679	234.047	17.119	0.000
Basic density	-13.52	2.265	6.573	0.004
Tracheid length	8.440	1.173	4.943	0.004
Wood ray proportion	-0.170	0.028	3.101	0.027
Tracheid proportion	0.504	0.101	3.719	0.06

Table 9. ANOVA (analysis of variance) Table for MOE

Model	quadratic sum	DOF	mean square	F distribution	significance
1 regression	547184.386	1	547184.386	6.189	0.038
residual	467963.634	10	77993.939		
total	1015148.020	11			
2 regression	659198.114	2	501419.934	7.016	0.027
residual	355949.906	9	61054.314		
total	1015148.020	11			
3 regression	773421.344	3	461306.057	10.004	0.010
residual	241726.676	8	47339.152		
total	1015148.020	11			
4 regression	855094.011	4	427547.006	13.356	0.004
residual	160054.009	7	32010.802		
total	1015148.020	11			

Table 10. Summary of Mathematical Model for Wood Veneer Tensile Strength

Model	correlation coefficient R	R ²	Standard error
1	0.778	0.605	2.30184
2	0.843	0.713	1.90051
3	0.958	0.918	1.23364
4	0.991	0.982	0.61783

Table 11. Regression Coefficient Table for Wood Veneer Tensile Strength

Model	correlation coefficient		t	significance
	Beta	Standard error		
1 constant	-98.363	10.885	-9.037	0.0001
Basic density	422.291	33.210	12.716	0.000015
2 constants	-67.630	14.616	-4.069	0.010
Basic density	342.78	54.278	4.990	0.004
Tracheid length	3.649	1.040	3.040	0.029
3 constants	-59.471	11.495	-7.247	0.0007
Basic density	270.872	40.047	8.102	0.004
Tracheid length	3.025	0.716	8.359	0.007
Tracheid proportion	4.905	1.152	3.302	0.009
4 constants	-63.060	7.375	-8.551	0.001
Basic density	212.827	30.828	6.904	0.002
Tracheid length	3.844	0.961	6.794	0.002
Tracheid proportion	4.138	1.030	3.992	0.016
Crystallinity	0.463	0.127	3.508	0.007

Table 12. ANOVA (analysis of variance) Table for Wood Veneer Tensile Strength

Model	Quadratic sum	DOF	mean square	F distribution	Significance
1 regression	584.008	1	584.008	161.689	0.00015
residual	21.672	10	3.612		
total	605.680	11			
2 regression	593.261	2	299.035	196.491	0.00018
residual	12.419	9	1.522		
total	605.680	11			
3 regression	601.060	3	240.805	231.363	0.00016
residual	4.62	8	0.799		
total	605.680	11			
4 regression	604.153	4	201.384	527.581	0.00012
residual	1.527	7	0.382		
total	605.680	11			

According to Tables 10, 11, and 12, it can be concluded that the most effective anatomical parameters to wood veneer tensile strength (y_3) include basic density (x_1), tracheid length (x_2), tracheid proportion (x_7), and crystallinity (x_{10}). The mathematical model concluded is given as Eq. 9:

$$y_3 = 212.83x_1 + 3.84x_2 + 0.46x_7 + 4.13x_{10} - 63.06 \quad (9)$$

CONCLUSIONS

In this study, several mathematical regression equations were established to reveal the general rule of each anatomical, physical, and mechanical properties.

1. From 1 to 17 annual rings, tracheid length increased rapidly at first, and then it increased slowly, belonging to type I (Pashin); tracheid length to width ratio also showed an overall increasing trend with the increase of annual ring age, and there was a certain fluctuation. Tracheid width and tracheid double wall thickness showed a slight increasing trend with the increase of annual ring age, and slightly decreased or tended to be flat after the 13th annual ring. The other tracheid morphological indexes had no obvious radial variation. Among clones, the difference of tracheid double wall thickness was significant at the $\alpha = 0.1$ level. There were significant differences in tracheid width and tracheid wall to cavity ratio. There was no significant difference in tracheid length and tracheid length to width ratio.
2. The basic density of plantation tree *Cunninghamia lanceolata* increased from pith heart center to bark within-clone. At the level of $\alpha = 0.1$, basic density was not significant between-clones. Crystallinity, MOR, and MOE in sapwood was larger than that of heartwood, and the variation was not significant within-clone and between-clones. Wood veneer tensile strength increased with increasing of growth ring age.

3. The multiple regression equations between MOR (y_1), MOE (y_2), Wood veneer tensile strength (y_3), and each anatomical factor established by variance analysis method were: $y_1 = 17.001x_1 + 2.433x_3 + 7.92x_6 + 14.237x_7 + 7.457x_{10} - 47.824$; $y_2 = 4006.679 - 13.52x_1 + 8.44x_2 + 0.504x_7 - 0.17x_8$; $y_3 = 212.83x_1 + 3.84x_2 + 0.46x_7 + 4.13x_{10} - 63.06$. Considering that the four clones were cultivated under specific conditions in Kaihua County Tree Farm, Zhejiang Province, the current formula has guiding significance for the four clones, and the promotion of the formula needs further research.
4. Since the four clones mainly contain tracheids having lengths greater than 3000 μm from the 8th annual ring, and then the length increases gradually, it can be inferred that the 8th to the 17th annual rings of wood in the experiment can be used as indicators of high-quality raw materials in the paper industry.

ACKNOWLEDGMENTS

Special thanks to following for their research support: The National Key Research and Development Program of China (2017YFD0600202); National Natural Science Foundation of China (31860184); Young Talents of Science and Technology in Universities of Inner Mongolia Autonomous Region NJYT-20-A15; Inner Mongolia science and technology major projects (CGZH2018135); and Inner Mongolia grassland talent team, innovative talent team (TC2019071720712).

REFERENCES CITED

- Almeida, D. H., Cavaleiro, R. S., Ferro, F. S., Almeida, T. H., Christoforo, A. L., Junior, C. C., and Lahr, F. A. R. (2014). "Modulus of elasticity of *Schizolobium amazonicum* wood evaluated by transversal vibration technique," *Wood Science and Technology* 912-914, 247-250. DOI: 10.4028/www.scientific.net/amr.912-914.247
- Amera, M., Kabouchia, B., Rahoutib, M., Famiric, A., Fidahc, A., and Alamia, S. (2005). "Influence of moisture content on the axial resistance and modulus of elasticity of clonal eucalyptus wood," in: *The Scientific Committee of the International Conference on Materials and Environmental Science*, Amsterdam, Netherlands, pp. 562-568.
- Adey-Johnson, R., Mclean, J. P., Bulcke, J. V. D., Acker, J. V., and McDonald, P. J. (2020). "Micro-CT measurements of within-ring variability in longitudinal hydraulic pathways in Norway spruce," *International Association of Wood Anatomists* 41 (1), 12-29. DOI: 10.1163/22941932-00002104
- Abdel-Aal, M. A., Nasser, R. A., Khan, P. R., and Al-Mefarrej, H. A. (2015). "Anatomical and physical characterisations of some lignocellulosic residues and their suitability for fibre production," *Journal of environmental biology* 36, 543-549.
- Bailleres, H., Vitrac, O., and Ramanantoandro, T. (2005). "Assessment of continuous distribution of wood properties from a low number of samples: Application to the variability of modulus of elasticity between trees and within a tree," *Holzforschung* 59, 524-530. DOI: 10.1515/HF.2005.0

- Babiak, M., Gaff, M., Sikora, A., and Hysek, Š. (2018). "Modulus of elasticity in three- and four-point bending of wood," *Composite Structures* 204, 454-465. DOI: 10.1016/j.compstruct.2018.07.113
- Barrett, J. D., and Hong, J. (2010). "Moisture content adjustments for dynamic modulus of elasticity of wood members," *Wood Science and Technology* 44, 485-495. DOI: 10.1007/s00226-009-0292-z
- Cabardo, S. J., Langrish, T. A. G., Dickson, R., and Joe, B. (2006). "Variability in transport properties regarding drying behavior for blackbutt timber in New South Wales," *Drying Technology* 24(2), 211-224. DOI: 10.1080/07373930600559167
- Cabardo, S. J., Langrish, T. A. G., Dickson, R., and Joe, B. (2007). "Variability in mechanical and drying properties for blackbutt timber in New South Wales," *Journal of the Institute of Wood Science* 17(6), 311-326. DOI: 10.1179/wsc.2007.17.6.311
- Crous, J. W., Morris, A. R., and Scholes, M. C. (2009). "Effect of phosphorus and potassium fertiliser on stem form, basic wood density and stem nutrient content of *Pinus patula* at various stem heights," *Australian Forestry* 72(2), 99-111. DOI: 10.1080/00049158.2009.10676295
- Deng, X., Zhang, L., Lei, P., Xiang, W., and Yan, W. (2014). "Variations of wood basic density with tree age and social classes in the axial direction within *Pinus massoniana* stems in Southern China," *Annals of Forest Science* 71(4), 505-516. DOI: 10.1007/s13595-013-0356-y
- Diesel, K. M. F., Costa, F. S. L., Pimenta, A. S., and Lima, K. M. G. (2014). "Near-infrared spectroscopy and wavelength selection for estimating basic density in *Mimosa tenuiflora* [Willd.] Poiret wood," *Wood Science and Technology* 48, 949-959. DOI: 10.1007/s00226-014-0652-1
- Derikvand, M., Kotlarewski, N., Lee, M., Hui, J., Chan, A., and Nolan, G. (2019). "Short-term and long-term bending properties of nail-laminated timber constructed of fast-grown plantation eucalypt," *Construction and Building Materials* 211, 952-964. DOI: 10.1016/j.conbuildmat.2019.03.305
- Derikvand, M., Kotlarewski, N., Lee, M., Hui, J., and Nolan, G. (2018). "Flexural and visual characteristics of fibre-managed plantation *Eucalyptus globulus* timber," *Wood Material Science & Engineering* 15(3), 172-181. DOI: 10.1080/17480272.2018.1542618
- GB/T 1933 (2009). "Method for determination of the density of wood," Standardization Administration of China, Beijing, China.
- GB/T 1936.1 (2009). "Method of testing in bending strength of wood," Standardization Administration of China, Beijing, China.
- Guan, C., Liu, J., Zhang, H., Wang, X., and Zhou, L. (2019). "Evaluation of modulus of elasticity and modulus of rupture of full-size wood composite panels supported on two nodal-lines using a vibration technique," *Construction and Building Materials* 218, 64-72. DOI: 10.1016/j.conbuildmat.2019.05.086
- Hauksson, J. B., Bergqvist, G., Bergsten, U., Sjöström, M., and Edlund, U. (2001). "Prediction of basic wood properties for Norway spruce. Interpretation of near infrared spectroscopy data using partial least squares regression," *Wood Science and Technology* 35, 475-485. DOI: 10.1007/s00226-001-0123-3
- Havimo, M. (2010). "Control of tracheid cross-sectional dimensions in Norway spruce and Scots pine wood raw material," *Scandinavian Journal of Forest Research* 25, 462-469. DOI: 10.1080/02827581.2010.509327

- Ivkovic, M., and Rozenberg, P. (2004). "A method for describing and modelling of within-ring wood density distribution in clones of three coniferous species," *Annals of Forest Science* 61, 759-769. DOI: 10.1051/forest:2004072
- Jones, P. D., Schimleck, L. R., Peter, G. F., Daniels, R. F., and Clark, III, A. (2005). "Non-destructive estimation of *Pinus taeda* L. tracheid morphological characteristics for samples from a wide range of sites in Georgia," *Wood Science and Technology* 39, 529-545. DOI: 10.1007/s00226-005-0021-1
- Liang, L., Fang, G., Deng, Y., Xiong, Z., and Wu, T. (2019). "Determination of moisture content and basic density of poplar wood chips under various moisture conditions by near-infrared spectroscopy," *Forest Science* 65(5), 548-555. DOI: 10.1093/forsci/fxz007
- Lima, J. T., Breese, M. C., and Cahalan, C. M. (2000). "Genotype-environment interaction in wood basic density of *Eucalyptus* clones," *Wood Science and Technology* 34, 197-206. DOI: 10.1007/s002260000041
- Liu, Y., and Zhao, G. (2012). *Wood Science*, Vol. 1, 2nd Ed., China Forestry Publishing House, Beijing, China.
- Locosselli, G. M., and Ceccantini, G. (2012). "Plasticity of stomatal distribution pattern and stem tracheid dimensions in *Podocarpus lambertii*: an ecological study," *Annals of Botany* 110, 1057-1066. DOI: 10.1093/aob/mcs179
- Moshtaghin, A. F., Franke, S., Keller, T., and Vassilopoulos, A. P. (2016). "Experimental characterization of longitudinal mechanical properties of clear timber: Random spatial variability and size effects," *Construction and Building Materials* 120, 432-441. DOI: 10.1016/j.conbuildmat.2016.05.109
- Olaoye, K., and Okon-Akan, O. A. (2020). "Estimation of modulus of elasticity of *Boscia angustifolia* wood using longitudinal vibration acoustic method," *International Wood Products Journal* 11(3), 122-128. DOI: 10.1080/20426445.2020.1738118
- Ona, T., Sonoda, T., Shibata, K. I. M., Kato, T., and Ootake, Y. (1998). "Determination of wood basic density by Fourier transform raman spectroscopy," *Journal of Wood Chemistry and Technology* 18(3), 367-379. DOI: 10.1080/02773819809349586
- Pangh, H., Hosseinabadi, H. Z., Kotlarewski, N., Moradpour, P., Lee, M., and Nolan, G. (2019). "Flexural performance of cross-laminated timber constructed from fibre-managed plantation eucalyptus," *Construction and Building Materials* 208, 535-542. DOI: 10.1016/j.conbuildmat.2019.03.010
- Pommier, R., Breyse, D., and Garbay, G. (2014). "Modelling the distribution of the variability of Maritime Pine for wooden sawn timber and finger jointing," *European Journal of Environmental and Civil Engineering* 18(6), 669-682. DOI: 10.1080/19648189.2014.908652
- Passialis, C. N. (1998). "A comparison of two methods for determining the basic density of small irregular samples of old waterlogged wood," *European Journal of Wood and Wood Products* 56(1), 91-92. DOI: 10.1007/s001070050273
- Pashin, A. J., and Zeeuw, C. (1980). *Textbook of Wood Technology*, Vol. 1, 3rd Ed., McGraw Hill, New York, USA.
- Raymond, C. A., and Muneri, A. (2001). "Nondestructive sampling of *Eucalyptus globulus* and *E. nitens* for wood properties. I. Basic density," *Wood Science and Technology* 35, 27-39. DOI: 10.1007/s002260000078
- Soriano-Luna, M. Á., Ángeles-Pérez, G., Guevara, M., Birdsey, R., Pan, Y., Vaquera-Huerta, H., Valdez-Lazalde, J. R., Johnson, K. D., and Vargas, R. (2018). "Determinants of above-ground biomass and its spatial variability in a temperate

- forest managed for timber production,” *Forests* 9(8), Article Number 490. DOI: 10.3390/f9080490
- Schimleck, L. R., and Evans, R. (2004). “Estimation of *Pinus radiata* D. Don tracheid morphological characteristics by near infrared spectroscopy,” *Holzforschung* 58, 66–73. DOI: 10.1515/HF.2004.009
- Schimleck, L. R., Jones, P. D., Peter, G. F., Daniels, R. F., and Clark, III, A. (2004). “Nondestructive estimation of tracheid length from sections of radial wood strips by near infrared spectroscopy,” *Holzforschung* 58, 375–381. DOI: 10.1515/HF.2004.057
- Schimleck, L. R., Mora, C., and Daniels, R. F. (2006). “Characterization of the cellulosic cell wall,” in: *Rapid Estimation of Tracheid Morphological Characteristics of Green and Dry Wood by Near Infrared Spectroscopy*, Douglas D., Leslie H. (ed.), Wiley-Blackwell, Hoboken, NJ, USA, pp. 95-109.
- Schimleck, L., Antony, F., Dahlen, J., and Moore, J., (2018). “Wood and fiber quality of plantation-grown conifers: A summary of research with an emphasis on loblolly and radiata pine,” *Forests* 9, 298. DOI: 10.3390/f9060298
- Searle, S. D., and Owen, J. V. (2005). “Variation in basic wood density and percentage heartwood in temperate Australian *Acacia* species,” *Australian Forestry* 68(2), 126-136. DOI: 10.1080/00049158.2005.10674956
- Sseremba, O. E., Mugabi, P., Banana, A. Y., Wessels, B. C., and Plessis, M. (2020). “Variation of basic density, calorific value and volumetric shrinkage within tree height and tree age of Ugandan grown *Eucalyptus grandis* wood,” *Journal of Forestry Research* 32, 503-512. DOI: 10.1007/s11676-020-01141-7
- Townshend, E., Pokharel, B., Groot, A., Pitt, D., and Dech, J. P. (2015). “Modeling wood fibre length in black spruce (*Picea mariana* (Mill.) BSP) based on ecological land classification,” *Forests* 6, 3369-3394. DOI: 10.3390/f6103369
- Vestøl, G. I., Høibø, O., Langsethagen, K. G., Skaug, E., and Skyrud, R. E. A. (2012). “Variability of density and bending properties of *Picea abies* structural timber,” *Wood Material Science & Engineering* 7(2), 76-86. DOI: 10.1080/17480272.2012.662698
- Vikberg, T., and Elustondo, D. (2015). “Basic density determination for Swedish softwoods and its influence on average moisture content of wood packages estimated by measuring their mass,” *Wood Material Science & Engineering* 11(4), 248-253. DOI: 10.1080/17480272.2015.1090481
- Vaganov, E. A., Schulze, E., Skomarkova, M. V., Knohl, A., Brand, W. A., and Roscher, C. (2009). “Intra-annual variability of anatomical structure and $\delta^{13}\text{C}$ values within tree rings of spruce and pine in alpine, temperate and boreal Europe,” *Oecologia* 161, 729-745. DOI: 10.1007/s00442-009-1421-y
- Wang, S., Lin, C., and Chiu, C. (2003). “The adjusted dynamic modulus of elasticity above the fiber saturation point in Taiwan plantation wood by ultrasonic-wave measurement,” *Holzforschung* 57, 547-552. DOI: 10.1515/HF.2003.081
- Watt, M. S., D’Ath, R., Leckie, A. C., Clinton, P. W., Coker, G., Davis, M. R., Simcock, R., Parfitt, R. L., Dando, J., and Mason, E. G. (2008). “Modelling the influence of stand structural, edaphic and climatic influences on juvenile *Pinus radiata* fibre length,” *Forest Ecology and Management* 254, 166-177. DOI: 10.1016/j.foreco.2007.07.036
- Watt, M. S., and Trincado, G. (2019). “Modelling the influence of environment on basic density of the juvenile wood for *Pinus radiata* grown in Chile,” *Forest Ecology and Management* 448, 112-118. DOI: 10.1016/j.foreco.2019.06.001

- Wu, Z., Zhou, C., Zhou, X., Hu, X., and Gan, J. (2018). "Variability after 15 years of vegetation recovery in natural secondary forest with timber harvesting at different intensities in southeastern China: Community diversity and stability," *Forests* 9(1), article no. 40. DOI: 10.3390/f9010040
- Yu, H., Liu, Y., Han, G., and Cui, Y. (2009). "Comparison of image analysis and conventional methods for cellular tissue proportion measurement of wood," in: *Proceedings of the 2009 IEEE: International Conference on Information and Automation*, Zhuhai/Macau, China.
- Yarnan, B. (2007). "Comparative wood anatomy of *Pinus sylvestris* and its var. *compacta* in the West Black Sea Region of Turkey," *International Association of Wood Anatomists* 28(1), 75-82. DOI: 10.1163/22941932-90001620
- Zhang, P., Wu, F., and Kang, X. (2011). "Differences in fiber properties and basic wood density in triploid hybrids of *Populus tomentosa*," *Advanced Materials Research* 236-238, 1442-1452. DOI: 10.4028/www.scientific.net/AMR.236-238.1442
- Zhu, J.Y., Scott, C. T., Scallan, K. L.; and Myers, G. C. (2006). "Using ring width correlations to study the effects of plantation density on wood density and anatomical properties of red pine (*Pinus resinosa* Ait.)," in: *3rd International Symposium on Emerging Technologies of Pulp and Papermaking*, Guangzhou, China, pp. 63-71.

Article submitted: January 23, 2021; Peer review completed: March 14, 2021; Revised version received and accepted: March 21, 2021; Published: March 25, 2021.

DOI: 10.15376/biores.16.2.3494-3519